Available online at www.sciencedirect.com
SCIENCE DIRECT
Surface & Coatings Technology 200 (2006) 4564 – 4571
SURFACE & COATINGS TECHNOLOGY
www.elsevier.com/locate/surfcoat

Influence of film structure and composition on diffusion barrier performance of SiO_x thin films deposited by PECVD

A. Grüniger[a], A. Bieder[a], A. Sonnenfeld[a], Ph. Rudolf von Rohr[a,*], U. Müller[b], R. Hauert[b]

[a]Swiss Federal Institute of Technology (ETH) Zurich, Institute of Process Engineering, Zurich CH-8092, Switzerland
[b]Empa, Materials Science and Technology, Überlandstrasse 129, Dübendorf CH-8600, Switzerland

Received 10 February 2005; accepted in revised form 30 March 2005
Available online 23 May 2005

Abstract

This study focuses on the oxygen permeability of SiO_x thin films on polyethyleneterephtalate (PET) produced by plasma-enhanced chemical vapor deposition (PECVD) from oxygen-diluted hexamethyldisiloxane (HMDSO). The versatile PECVD set-up, equipped with two plasma sources (remote microwave and direct radio frequency), allows the deposition of films with variable morphologies and compositions. The deposits were analyzed by XPS, ellipsometry, and atomic force microscopy (AFM). Curve fitting of the Si 2p peak in X-ray photoelectron spectra (XPS) provided information about the chemical binding states of the silicon atoms. The results clearly show that the oxygen transmission rate (OTR) depends highly on the film structure, whereas the chemical composition has only little effect.

In order to achieve the desired dense and smooth film structure, it is necessary to have a high substrate bias, which promotes ion bombardment of the film surface during growth. OTR values down to 0.2 cm^3 (STP) m^{-2} day^{-1}, corresponding to a barrier improvement factor of 500, have been achieved.

Keywords: Silicon oxide barrier coatings; Plasma-enhanced chemical vapour deposition (PECVD); Microwave; RF; X-ray photoelectron spectroscopy (XPS); Atomic force microscopy (AFM)

1. Introduction

Nano-sized, amorphous SiO_x films receive considerable attention in packaging industry due to their excellent diffusion barrier performance. The main advantages of these films compared to metallic films are their optical transparency, recyclability, and suitability for microwaving [1]. Common deposition techniques for SiO_x films are based on physical vapor deposition (PVD) or plasma-enhanced chemical vapor deposition. PVD processes comprise evaporation or sputtering of a solid precursor (Si, SiO, and SiO_2). In contrast, PECVD processes use volatile organo-silicon precursors, which become excited and partially decomposed in the plasma [2]. Therefore, PECVD opens up a chemical pathway to precisely control polymerization and deposition process by means of external plasma parameters. Thus, compared to PVD methods, it can yield strong chemical bonding [3,4]. Moreover, it enables three-dimensional coating, while PVD techniques are restricted to line-of-sight deposition.

Reviews on SiO_x barrier film deposition on flexible polymeric webs, in particular on PET, are given in [1,5,6]. With regard to application, deposition on PET bottles [7] and on paper-based substrates [8] has been reported. In the future, improved multi-barrier film systems for moisture protection of organic-based display technologies (OLED displays) will be an emerging field of application [9], where the barrier effect of coatings will still have to be improved by orders of magnitude.

This study focuses on the oxygen permeability of SiO_x films deposited on PET, produced by PECVD from oxygen-diluted hexamethyldisiloxane (HMDSO). In consequence of the non-equilibrium character of plasma chemical reactions, the barrier film performance depends on the apparatus being

* Corresponding author. Tel.: +41 44 632 24 88; fax: +41 44 632 13 25.
E-mail address: vonrohr@ipe.mavt.ethz.ch (Ph. Rudolf von Rohr).

0257-8972/$ - see front matter © 2005 Elsevier B.V. All rights reserved.
doi:10.1016/j.surfcoat.2005.03.044

used. It is the intention of this work to investigate the influence of barrier film structure and composition and, thus, to provide "system-independent" information necessary to optimize the barrier performance of SiO_x films.

2. Experimental

2.1. PECVD set-up

A schematic drawing of the experimental set-up is shown in Fig. 1. The PECVD apparatus consists of a cylindrical reactor made of stainless steel. On its top, a microwave (MW) resonator is mounted. It is driven by a magnetron operating at a frequency of 2.45 GHz. By means of slot antenna in the inner wall of the resonator (SLAN I [10]), microwaves are coupled into a quartz cylinder (∅ 160 mm), which equals the diameter of the reactor following downwards (gas stream orientation). The total reactor volume amounts to 20 l. The substrate is positioned on a length-variable substrate holder, which is capacitively coupled, via a matching network, to a radio frequency (RF) generator, working at 13.56 MHz. In order to avoid plasma formation at the backside of the substrate holder, a dark space shield is used. Oxygen is introduced at the top of the reactor, while HMDSO is fed in through a wall-integrated shower, 95 mm below the SLAN bottom.

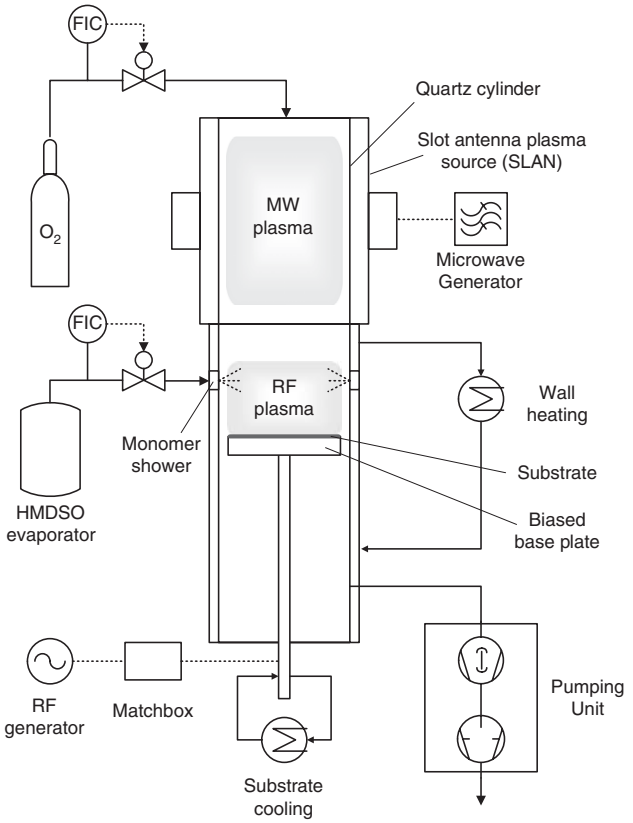

Fig. 1. Scheme of the PECVD set-up.

Table 1
Reference conditions of the different plasma source operation modes for film deposition

Process parameters	Mode		
	MW	RF	Dual
MW power P_{MW} [W]	1500		1500
RF power input P_{RF} [W]		200	200
Pressure [mbar]	0.14	0.2	0.2
HMDSO flow rate [sccm]	10	10	10
Oxygen flow rate [sccm]	400	150	150
Ratio of the oxygen and HMDSO flow rate q	40	15	15
Substrate temperature [°C]	70	20	20
Distance Substrate SLAN [mm]	245	245	245
Deposition time [s]	120	60	60
Self-bias U_b [V]		−589	−634

Both plasma sources can be operated independently. In the following, the *MW mode* will refer to the mode of operation with microwave plasma excitation only. Analogous, *RF mode* refers to RF generator operation only, and *dual mode* stands for MW and RF operation, simultaneously. Determined for each mode in preliminary tests, the optimal process conditions are in the following referred to as *reference conditions*, listed in Table 1. They are close to optimum in terms of low oxygen permeability of the deposited films. Regarding RF and dual mode, the reference conditions are almost the same but differ for MW mode because the latter corresponds to a remote process. Starting from these reference conditions, the parameters were varied individually while keeping the others constant in order to investigate the influence of a single parameter.

When RF power is applied to the substrate holder, a negative DC self-bias voltage U_b, measured between the substrate base plate and the grounded reactor walls, develops. In Fig. 2, it is clearly shown that the value of U_b depends mainly on the RF power input $P_{RF}=P_{fwd}-P_{refl}$, with P_{fwd} being the generator forward power and P_{refl} being the power reflected from the substrate holder. Variations in U_b of about ±5% may occur.

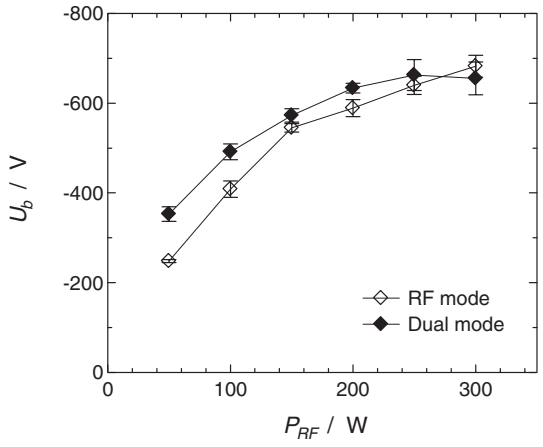

Fig. 2. Substrate self-bias as a function of RF power input.

2.2. Film characterization

2.2.1. Oxygen transmission rate

In order to measure oxygen permeability, the SiO_x films were deposited on PET films of 12 μm thickness (Type Mylar, DuPont Teijin Films). The oxygen transmission rate (OTR) of the composites was measured by a permeability tester (Ox-Tran 100, Mocon Inc.) according to DIN 53380-3 at 25 °C. The detection limit of this method is 0.1 cm^3 (STP) m^{-2} day^{-1}.

2.2.2. X-ray photoelectron spectroscopy (XPS)

For the XPS measurements on the SiO_x films, deposition experiments have been conducted using pieces of Si(100) wafers as substrates. In order to determine the concentration and chemical status of silicon, oxygen, and carbon in the deposited films, XPS spectra were acquired on a Physical Electronics (PHI) Quantum 2000 photoelectron spectrometer. The samples were exposed to a monochromatized X-ray beam (Al $K\alpha = 1486.6$ eV). Low-energy electrons and argon ions were used simultaneously to compensate for electrical charging of insulating surface areas during analysis. Emitted photoelectrons were analyzed with a hemispherical electron energy analyzer equipped with a channel plate and a position sensitive detector. The electron take-off angle was 45°; the analyzer was operated in the constant pass energy mode at 58.7 eV, giving a total energy resolution of 1.05 eV. The binding energy scale of the analyzer was calibrated for the Au 4f electrons to be at 84.0 eV ± 0.1 eV. The residual background pressure inside the spectrometer was lower than 5×10^{-9} mbar during analysis. Elemental concentrations are given in atomic percent (normalized to a total of 100 at.%) using the photoelectron peak areas after Shirley background subtraction (Multi-Pack, Version 6.1, Physical Electronics Inc., Eden Prairie, MN, USA) and built-in PHI sensitivity factors for the calculation.

To remove adventitious carbon as well as a natural SiO_2 surface oxide layer, prior to analysis, the sample surfaces have been cleaned by 4 kV argon ion bombardment. Different argon ion cleaning durations between 6 s and 30 s, corresponding to the removal of 2 nm to 10 nm of material (on a SiO_2 reference film), did result in identical XPS spectra.

Due to residual charging of the samples during analysis, the actual peak positions had to be referenced to the Ar 2p peak at 241.9 eV.

2.2.3. Atomic force microscopy (AFM)

The surface morphology of the films deposited on Si(100) wafers was visualized by means of atomic force microscopy. A multimode scanning microscope with NanoScope IIIa controller (Veeco Metrology Group) was used. Areas of 1×1 μm^2 were scanned in tapping mode in ambient air. After plane fitting, the root mean square roughness R_q was calculated from the height profile $z(x)$ according to:

$$R_q = \sqrt{\frac{1}{n}\sum (z_i - \bar{z})^2}$$

where $\bar{z}$ is the mean height and n is the number of data points.

2.2.4. Ellipsometry

A variable angle spectroscopic ellipsometer (M-2000F, J.A. Woollam Inc.) was used to measure the film thickness. Measurements were performed at three different incident angles (65°, 70°, and 75°) in the range of 245 nm–995 nm. The wavelength dependence of the refractive index was approximated by a Cauchy model. Combination with gravimetric measurements allowed determination of the film density.

3. Results and discussion

3.1. Comparison of deposition modes

Fig. 3 shows a comparison of OTR values of PET samples coated in the different operation modes (at reference conditions) plotted over the film thickness. While there is no difference of barrier performance observed for RF- and dual-mode samples, the OTR values for MW-mode samples are significantly higher. Similar results have been found by Sobrinho et al. [11]. They attributed the lower transmission rates for RF mode and dual mode to the densifying effect of the ion bombardment caused by self-bias, which occurs when the substrate holder is RF-powered. This is confirmed by our film density results shown in Table 2. The MW samples, produced at reference

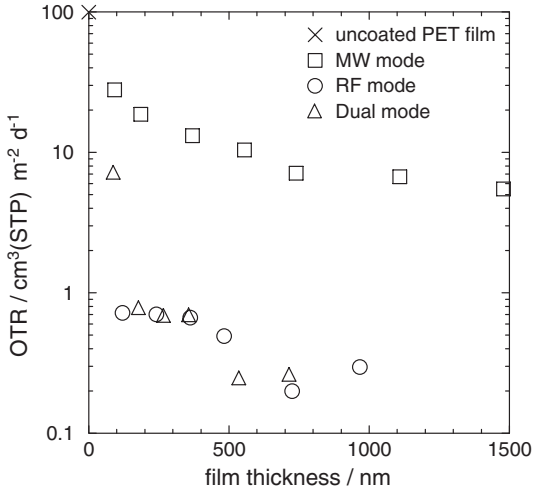

Fig. 3. Oxygen transmission rate (OTR) of deposits on PET vs. film thickness: comparison of plasma operation modes. Process conditions according to Table 1.

Table 2
Properties of SiO_x films deposited at different values of the RF power input P_{RF} and the oxygen-to-HMDSO ratio q

Plasma operation mode	Parameter of variation		Deposition rate [nm min^{-1}]	Film density [g cm^{-3}]	Surface roughness R_q [nm]	Carbon content [at.%]	OTR [cm^3 (STP) m^{-2} day^{-1}]
MW	None		185	1.80	4.11	1.2	11.7
RF	None		522	2.03	0.64	1.2	0.61
	P_{RF} [W]	50	461	1.49	0.69	8.6	89.0
		100	452	1.76	0.46		1.92
		300	474	2.08			0.38
	q	1			0.50	29.8	11.8
		2			0.41	19.7	2.63
		5	574	1.85	0.64	8.6	1.16
		30	513	2.12	0.80		0.46
Dual	None		391	2.05	6.89	0.6	0.65
	P_{RF} [W]	50	255	1.84	8.84	1.8	89.9
		100	373	2.01			14.2
		300	390	2.01			0.80
	q	1			0.51	40.9	2.70
		2			0.62	35.9	1.82
		5	384	1.81	8.94	8.0	1.03
		30	367	1.82	10.1		25.3

All other deposition parameters: *reference conditions* (Table 1).

conditions, exhibit a density of 1.80 g cm^{-3} compared to 2.03 g cm^{-3} and 2.05 g cm^{-3} for RF mode and dual mode, respectively. However, the different densities of films do not account for a significant change of their carbon content, as one might suspect. For all three modes, as found by means of XPS, the carbon content is rather low at reference conditions (Table 2).

In general, the deposition rates are the highest for RF mode and the lowest for MW mode. Because the substrate is positioned outside the active MW plasma zone, the energy transfer to the deposition zone from the MW plasma is limited by its distance to the substrate and by the oxygen flow rate, since atomic oxygen created in the MW plasma plays a major role as chemically exited carrier of the MW discharge energy [12]. Consequently, MW plasma operation reduces the deposition rate since film deposition takes also place at the reactor walls between MW source and deposition zone. We assume that this process also accounts for the lower deposition rates in dual mode compared to RF mode.

3.2. Variation of RF power

The variation of the RF power input P_{RF} has generally two aspects: it affects the plasma bulk properties and the gas phase reactions. Moreover, the self-bias voltage U_b increases with RF power as already shown in Fig. 2. The deposition rate (Table 2) does not significantly depend on P_{RF} within the observed range, with the exception that, in dual mode, it is lower for 50 W than for the other values of P_{RF} investigated. In contrast to the deposition rate, an increase of the film density with P_{RF} can be observed for both dual mode and RF mode (Table 2). In dual mode, the power-induced increase of film density is less pronounced because, in MW mode, the film density already attains 1.8 g cm^{-3}.

In RF mode, the density of films continuously increases from 1.49 g cm^{-3} to 2.08 g cm^{-3} with increasing P_{RF}. Although a simultaneous decrease of the carbon content of films from 8.6% for 50 W to about 1% at 200 W (reference conditions) is observed (Table 2), it makes up only a small portion of the density change. Since films with similar carbon content but lower density have been deposited in MW mode, the RF power-induced increase of the film density, in RF mode and dual mode, is a result of the increased ion bombardment due to the higher self-bias voltage U_b at higher values of P_{RF} (Fig. 2). Bombardment-induced bond break-up may lead to rearrangement and disruption of film growth structures and hence reduces porosity [13]. Consequently, it is likely that the continuous decrease of OTR with increasing P_{RF}, as shown in Fig. 4 for RF and dual mode, is mainly caused by the denser film structure.

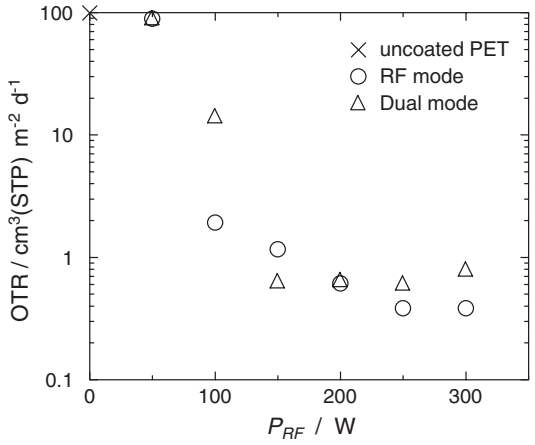

Fig. 4. Oxygen transmission rate (OTR) of deposits on PET vs. RF power input P_{RF}; other process parameters according to Table 1.

3.3. Variation of the oxygen flow rate

While keeping the flow rate of HMDSO constant at 10 sccm, the oxygen flow rate was varied such as to vary the oxygen-to-HMDSO ratio q in the range from 1 to 30. This parameter strongly affects film composition. Fig. 5 shows relative contents of the major elements as derived from XPS analysis for films deposited in RF mode and dual mode. The composition gradually turns from silicone-like to silica-like with increasing q in both operation modes. The carbon content converges to zero while the oxygen content approaches 67%. Thereby, the silicon concentration remains constant between 30% and 35%. The filled markers represent the composition of films deposited at P_{RF}=50 W (compared to 200 W for the others). As a result of the lower power input, the carbon content is raised, particularly for RF-mode samples. For dual mode, the film composition does not differ from films deposited in RF mode at P_{RF}=200 W.

Peak fitting of the Si 2p photoelectron signals was done analogous to reference [14]. In SiO_2, which has a tetragonal structure, the Si atom is bonded to four neighboring oxygen atoms and, therefore, we label it as Si(−O−)$_4$. The chemical shift in the Si 2p photoelectron signal is mainly induced by the number of oxygen atoms bound to a Si atom. When introducing carbon atoms into SiO_2, some of the four oxygen atoms bonded to the silicon are replaced by carbon atoms. The possible configurations, chemical states, are labeled Si(−O−)$_3$(−C−), Si(−O−)$_2$(−C−)$_2$, and Si(−O−)(−C−)$_3$. Of course, there would naturally be a fifth configuration, Si(−C−)$_4$, corresponding to silicon carbide, but which was not found in the films deposited. The Si 2p position of SiO_2 or quartz (Si(−O−)$_4$) at a binding energy of 103.4 eV, and of polydimethylsiloxane (PDMS) (Si(−O−)$_2$(−C−)$_2$) at a binding energy of 101.7 eV–102.1 eV, can be found in the literature [14,15]. The positions of Si(−O−)$_3$(−C−) and Si(−O−)(−C−)$_3$ have been reported to be at 102.6 eV–102.8 eV and 100.7 eV–101.5 eV binding energy, respectively, assuming a linear correlation between the chemical shift of the Si 2p signal and the number of oxygen atoms bonded to Si [14,15].

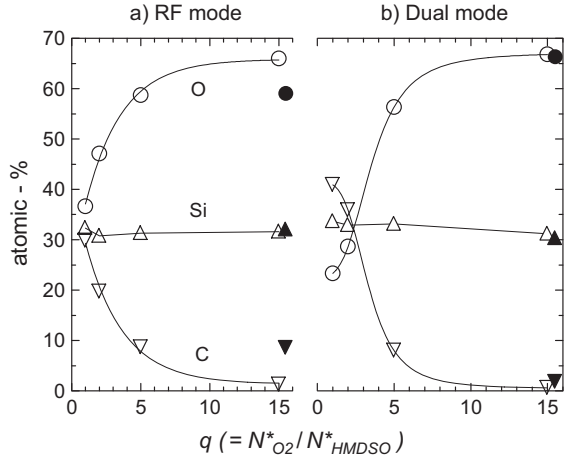

Fig. 5. XPS analysis: relative contents of major elements in the deposit with varying oxygen-to-HMDSO flow rate ratios q. Blank markers: P_{RF}=200 W; filled markers: P_{RF}=50 W.

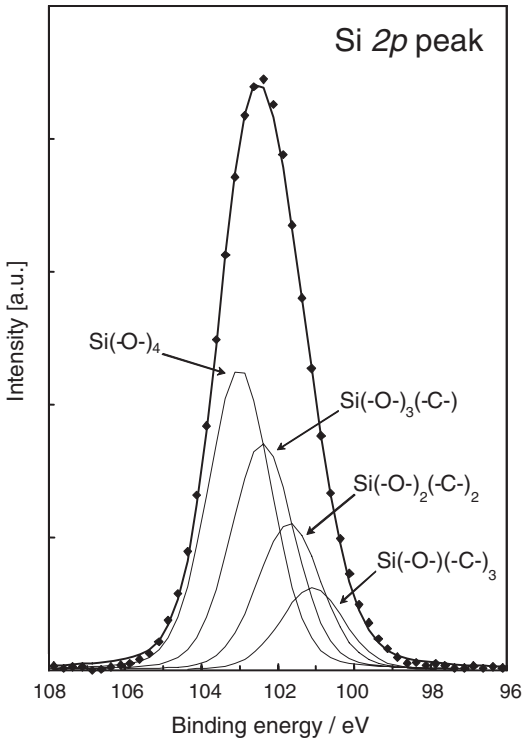

Fig. 6. XPS analysis: spectrum range of the Si 2p peak after background subtraction of a film deposited at P_{RF}=200 W and q=2 in RF mode; decomposition into the four chemical states: (Si(−O−)$_4$), Si(−O−)$_3$(−C−), Si(−O−)$_2$(−C−)$_2$, and Si(−O−)(−C−)$_3$.

In this work, the Si 2p peak fitting was done using fixed separations between the different chemical states (e.g., 0.6 eV, 1.3 eV, and 1.8 eV) relative to the Si(−O−)(−C−)$_3$ configuration for the Si(−O−)$_2$(−C−)$_2$, Si(−O−)$_3$(−C−), and (Si(−O−)$_4$ compounds, respectively. We obtained the best fits for peak position at 101.1 eV–101.3 eV for the Si(−O−)(−C−)$_3$ chemical state. The FWHM values varied between 1.97 eV and 2.2 eV. As an example, Fig. 6 shows the Si 2p peak after background subtraction of a film deposited in RF mode with an RF power input of P_{RF}=200 W and a oxygen-to-HMDSO ratio q=2. Furthermore, the decomposition into the four chemical states is presented. In this case, as in all others, the existence of a silicon carbide compound in the coatings obtained may be excluded, or may be at least below the detection limit of about 2 at.%. By this detailed peak analysis, we thus can deduce the amount of a single chemical state in the coatings and show its dependence on the film deposition parameters.

The results of all these Si 2p peak fits are shown in Fig. 7 (RF mode) and Fig. 8 (dual mode). Here, the dependence of the amount of the different chemical states of the silicon atoms on the amount of oxygen in the feed gas (ratio q) is shown. In both operation modes, a general increase in oxidation state with increasing oxygen flow rate can be

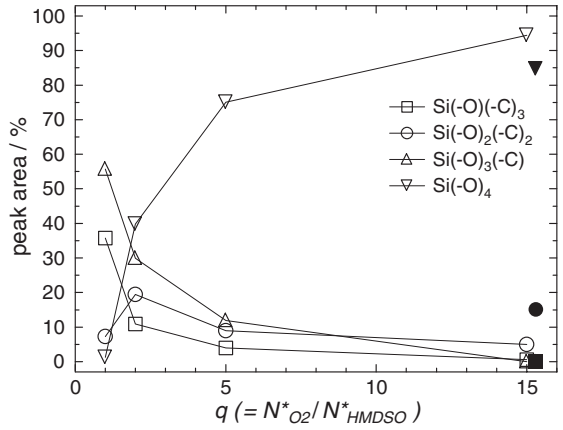

Fig. 7. XPS analysis: curve fit of Si 2p peak from deposits obtained in RF mode. Blank markers: P_{RF}=200 W; filled markers: P_{RF}=50 W.

observed. The Si(−O−)$_4$ peak, which corresponds to a silica network, converges to 100% at the expense of the other oxidation states. Si(−O−)(−C−)$_3$, the lowest oxidation state, equals the state of silicon in the HMDSO molecule. Its peak area makes up more than 80 % at q=1 for dual-mode deposition (Fig. 8). However, for RF-mode samples, at the same oxygen flow rate, it is already reduced to less than 40% (Fig. 7). Fig. 5 also shows that the total carbon content is lower at this deposition condition in RF mode. Although this phenomenon remains to be further investigated, we assume that the lower oxidation of films deposited in dual mode is evocated by the already addressed mechanism of film deposition occurring on the reactor walls between MW source and substrate. Obviously, this process reduces the effective oxygen flow and increases the flux of organo-silicon species (i.e., fragments of HMDSO as well as its oligomers) toward the deposition zone.

The latter, the formation of oligomers in the gas phase, is supported by our finding that the residual carbon at high oxygen flow rates (q=15) is mainly present as Si(−O−)$_2$(−C−)$_2$. This configuration corresponds to an oligomeric structure [16], which seems to be most stable apart from Si(−O−)$_4$.

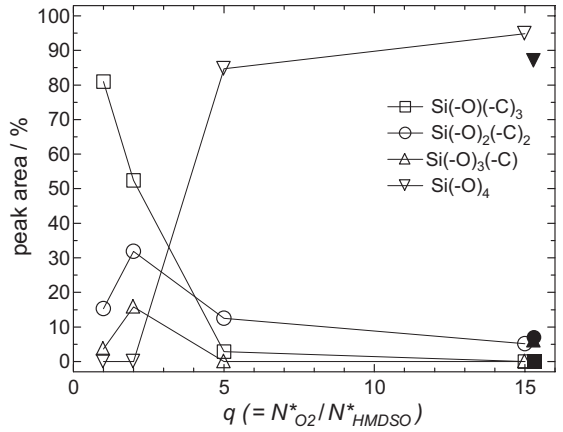

Fig. 8. XPS analysis: curve fit of Si 2p peak from deposits obtained in dual mode. Blank markers: P_{RF}=200 W; filled markers: P_{RF}=50 W.

Proper fitting of the ellipsometric measures was only possible for films with silica-like composition. Therefore, film deposition rates and densities are only available for $q \geq 5$ (Table 2). Within the observed range, the deposition rate does not significantly alter with q. The increase of film density between q=5 and q=15 is attributed to the changes of the chemical film composition. With higher values of q, the increase of density continues for RF mode but not for dual

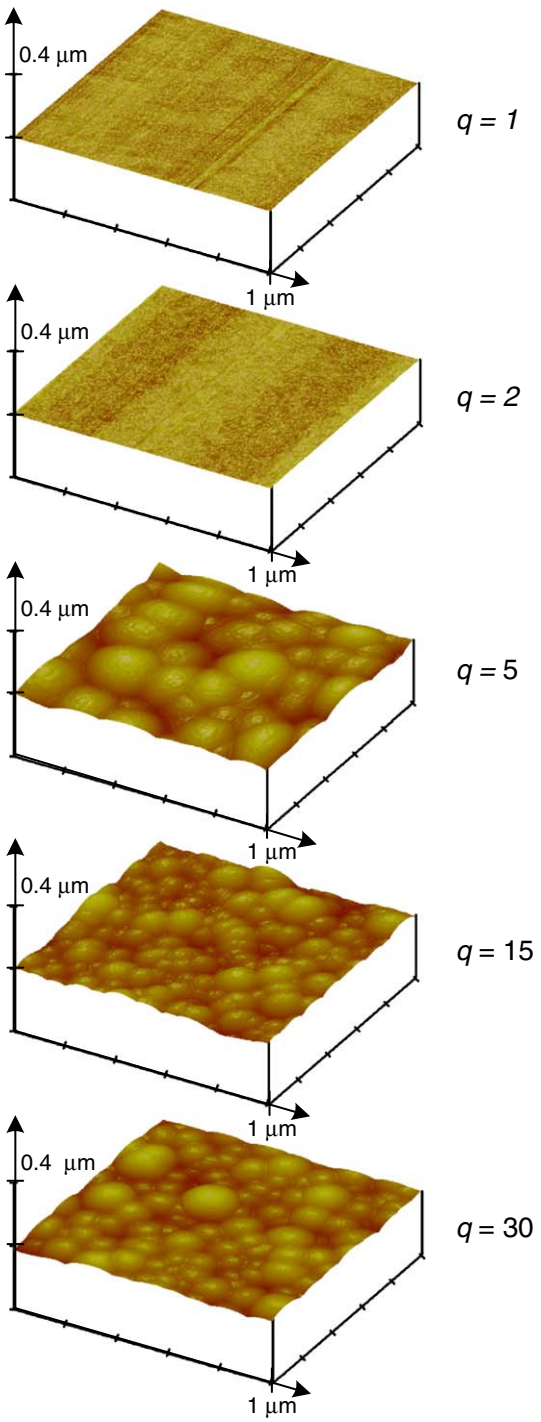

Fig. 9. AFM graphs of deposits formed in dual mode with varying oxygen-to-HMDSO flow rate ratios q.

mode, where the density is even reduced for $q=30$. This behavior is related to the film morphologies. The surface roughness values R_q are listed in Table 2. The atomic force micrographs in Fig. 9 illustrate the evolution of the film surface morphology with increasing oxygen flow rate in dual mode. Whereas all films deposited in RF mode exhibit, independently of q, a very smooth structure with a roughness below 1 nm, the film structure, in dual-mode series, changes from smooth to columnar with well-defined growth structures with an increase of q. In relying upon the revised structure zone model by Messier et al. [17], this finding indicates that film growth is governed by a reducing surface diffusion (mobility) of adsorbed species at increasing value of q.

Within the dual-mode series, the change of surface structures with increasing q (Fig. 9) can be explained with the decreasing amount of carbon containing structures of the films (Fig. 7). Since, the binding energy of the Si−C bond (4.53 eV) is much smaller than of the Si−O bond (8.31 eV), the ion bombardment of the surface is more efficient in disrupting growth structures if the carbon content is high.

Although the current results do not explain why these growth structures are absent in RF-mode deposits, it can be speculated that in contrast to dual mode, gas phase reactions of precursor derivatives are less important. Since the MW source is off in RF mode, initial precursor excitation (i.e., fragmentation) takes place closer to the substrate surface. Therefore, a larger number of excited fragments of HMDSO adsorb at the substrate. Since migration of the precursor fragments takes place more probably than heavier oligomeric adsorbates, the rearrangement of film growth structures is more likely in RF mode than in dual mode.

In any case, the comparison of the gas transmission rates provides valuable information on the structure–permeability relation of the films. Fig. 10 shows the OTR in dependence of the flow rate ratio q. The films deposited in RF mode exhibit continuously decreasing OTR values with increasing q and, hence, lowered carbon content. According to Lamendola and d'Agostino [18], a high carbon content promotes film formation at a low degree of cross-linking and high gas solubility. Nevertheless, in spite of more than 30% carbon content at $q=2$, the sample exhibits an OTR value below 3 cm^3 (STP) m^{-2} day^{-1}, which is still lower than the best value achieved for MW-mode deposited films with SiO_2-like structure (Fig. 3). In dual mode, the OTR rises again for q ratios higher than 15. This goes along with the discussed changes in film structure and the resulting decrease of film density.

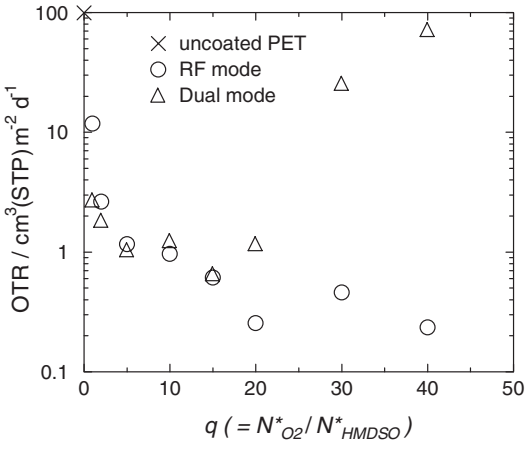

Fig. 10. Oxygen transmission rate (OTR) of deposits on PET vs. oxygen-to-HMDSO flow rate ratio q; other process parameters according to Table 1.

4. Conclusions

A versatile PECVD set-up has been used to deposit SiO_x diffusion barrier films from oxygen-diluted HMDSO. Thanks to the possibility of operating in three different modes (MW, RF, and dual), a broad range of deposits with variable morphology and composition has been produced.

The comparison of chemical composition and morphology of the deposited films clearly reveals a superior influence of the film structure upon oxygen transmission rate (OTR), whereas film composition has only little effect. Although a decreasing carbon content of films is accompanied by decreasing gas transmission rates, gas transmission is more sensitive to changes of film density and surface roughness.

Furthermore, it has been shown that a high substrate self-bias is favorable to achieve the desired dense and smooth film structure. Therefore, the higher oxygen permeability of MW-mode films is mainly attributed to the lack of a substrate bias. In RF mode, however, the electric field of the sample self-bias yields high-energy ion bombarding of the film surface, leading to bond breakage, inducing destruction of the film growth structures.

OTR values down to 0.2 cm^3(STP)m^{-2} day^{-1} have been reached within this study. This corresponds to a barrier improvement factor of 500. Czeremuszkin et al. [1] postulated an asymptotic residual value in the same order of magnitude (0.4 cm^3 (STP)m^{-2} day^{-1}) on the same type of PET substrate. It is likely that the limitation occurs due to dust and anti-block particles present on a PET film surface. For further improvement, special cleaning precautions and preparation of the substrate surface have therefore to be considered.

Acknowledgments

The authors wish to thank Prof. M. Textor and L. Feuz for their support in ellipsometry, and Prof. A. Stemmer and M. Sakai-Stalder for the AFM measurements. Furthermore, warm thanks goes to P. Hoffmann, B. Kramer, and B. Wellig for their help with the PECVD installation. In part, this project was supported by Cham Paper Group, Cham CH, and the Commission for Technology and Innovation (CTI), Bern, Switzerland.

References

[1] G.L. Czeremuszkin, M.R. Wertheimer, A.S. Da Silva Sobrinho, Plasmas Polym. 6 (1/2) (2001) 107.
[2] M. Ohring, The Materials Science of Thin Films, Academic Press, Boston, 1992.
[3] J.A. Thornton, J.E. Greene, in: R.F. Bunshah (Ed.), Handbook of Deposition Technologies for Films and Coatings—Science, Technology and Applications, Noyes Publications, Park Ridge, NJ, USA, 1994, p. 55.
[4] E.M. Liston, L. Martinu, M.R. Wertheimer, J. Adhes. Sci. Technol. 7 (10) (1993) 1091.
[5] H. Chatham, Surf. Coat. Technol. 78 (1–3) (1996) 1.
[6] Y. Leterrier, Prog. Mater. Sci. 48 (1) (2003) 1.
[7] K. Mueller, O_2-Durchlässigkeit von Kunststoffflaschen und Verschlüssen—Messung und Modellierung der Stofftransportvorgänge, Technische Universität München, München, 2003.
[8] A. Grüniger, Ph. Rudolf von Rohr, Surf. Coat. Technol. 174 (2003) 1043.
[9] A. Sugimoto, et al., IEEE J. Sel. Top. Quantum Electron. 10 (1) (2004) 107.
[10] D. Korzec, et al., Plasma Sources Sci. Technol. 5 (2) (1996) 216.
[11] A.S.D. Sobrinho, et al., J. Vac. Sci. Technol., A, Vac. Surf. Films 16 (6) (1998) 3190.
[12] C. Bayer, Ph. Rudolf von Rohr, Plasma Chem. Plasma Process. 18 (2) (1998) 189.
[13] L. Martinu, et al., J. Vac. Sci. Technol., A, Vac. Surf. Films 12 (4) (1994) 1360.
[14] M.R. Alexander, et al., Appl. Surf. Sci. 137 (1–4) (1999) 179.
[15] A. Barranco, et al., Surf. Coat. Technol. 180–81 (2004) 244.
[16] M.R. Alexander, F.R. Jones, R.D. Short, J. Phys. Chem., B 101 (18) (1997) 3614.
[17] R. Messier, A.P. Giri, R.A. Roy, J. Vac. Sci. Technol., A, Vac. Surf. Films 2 (2) (1984) 500.
[18] R. Lamendola, R. d'Agostino, Pure Appl. Chem. 70 (6) (1998) 1203.